Marine Geophysical Research (2021) 42:6
https://doi.org/10.1007/s11001-021-09427-z

ORIGINAL RESEARCH PAPER

Inverted long-baseline acoustic navigation of deep-towed CSEM transmitters and receivers

Kerry Key[1] · **Steven Constable**[2]

Received: 19 July 2020 / Accepted: 27 January 2021 / Published online: 15 February 2021

Abstract

We develop an inverted long-baseline (ILBL) acoustic navigation system for determining the position of deep-towed instruments, such as controlled-source electromagnetic transmitters and receivers. The ILBL system uses a deep-tow mounted acoustic transceiver system to measure travel times to a pair of surface transponders towed on paravanes behind the survey vessel. The travel times, transponder positions and pressure depth data are inverted for the lateral position of the deep-tow vehicle, as well as the positions of any relay transponders on the antenna and receiver array that are towed horizontal behind the deep-tow vehicle. Three example applications demonstrate position accuracies of about 5 and 37 m in the inline and crossline directions for 3 km water depths and around 6 m for 1 km depth. The portability and generality of the system make it suitable for deep-tow applications for geophysical, geochemical and geological surveying purposes. We have shown that the accuracy of the ILBL system is similar to that of commercial USBL systems, but is considerably more cost effective than even portable USBL systems, and can be used on vessels lacking permanently installed USBL transceiver heads. Further, it can be used in water depths of 5,000 m or more. It could also be readily modified for further improving its position accuracy if desired.

Keywords Marine electromagnetics · Long-baseline · Acoustic · Deep-tow · Navigation

Introduction

Marine controlled-source electromagnetic exploration

Our motivation to develop an improved marine navigation system arose from our use of marine controlled-source electromagnetic (CSEM) instruments, which generate data that are highly sensitive to relative instrument location. The CSEM method is a geophysical technique for mapping subsurface electrical conductivity using a deep-towed electric dipole source and an array of electromagnetic receivers that record the attenuation of the transmitted signal as a function of source position. In the deep ocean, CSEM data can constrain the fabric and hydration of the shallow lithosphere by mapping the depth dependence and azimuthal anisotropy of conductivity in the crust and upper-most mantle (e.g., Cox et al. 1986; Chesley et al. 2019). At mid-ocean ridges, CSEM profiling provides images of the crustal magmatic and hydrothermal systems (e.g., Johansen et al. 2019) and seafloor massive sulfide deposits (e.g,. Gehrmann et al. 2019b). At subduction zones, CSEM data can image crustal hydration and fluids in extentional bending faults on the incoming plate, and the structure and porosity in the forearc where the relative motion between the subducting and overriding plates occurs (e.g. Key et al. 2012; Naif et al. 2015, 2016). On the continental shelf, CSEM data have been used for offshore oil and gas exploration (e.g., Ellingsrud et al. 2002; Constable and Srnka 2007), for mapping seafloor gas hydrates (e.g., Schwalenberg et al. 2010; Weitemeyer et al. 2011; Attias et al. 2018; Kannberg and Constable 2020) and for studying submarine groundwater aquifers (Gustafson et al. 2019; Micallef et al. 2020).

In the typical marine CSEM application, a horizontal electric dipole transmitter is deep-towed behind a survey

✉ Kerry Key
kkey@ldeo.columbia.edu

Steven Constable
sconstable@ucsd.edu

[1] Lamont-Doherty Earth Observatory, Columbia University, Palisades, NY 10964, USA

[2] Scripps Institution of Oceanography, University of California San Diego, La Jolla, CA 92093-0225, USA

vessel at 20–100 m altitude above the seafloor while broadcasting low-frequency EM energy to an array of previously deployed ocean-bottom electromagnetic (OBEM) receivers, or to an array of receivers towed at distance behind the transmitter on a streamer cable. The magnitude and phase of the vector electric and magnetic fields recorded as a function of source and receiver position can be interpreted or inverted to obtain the sub-seafloor electrical conductivity structure. This electric dipole CSEM method is particularly sensitive to laterally extensive resistive bodies, even if very thin (e.g., Weidelt 2007), which proves particularly useful for offshore hydrocarbon exploration.

Since the transmitted CSEM fields decay exponentially with source–receiver range, one of the largest limitations in the interpretation and inversion of long-offset CSEM data is the uncertainty in the navigated positions of the transmitter and receivers (e.g., Gehrmann et al. 2019a). This strong range dependence and the azimuthal polarization of the transmitted field can be exploited to invert for the transmitter and receiver positions when independent navigation data are otherwise unavailable (Swidinsky and Edwards 2011; Weitemeyer and Constable 2014). However, such data-navigated positions can result in trade-offs with seafloor conductivity structure and thus it is preferable to independently navigate the system.

Such navigation must necessarily involve acoustic methods, since electromagnetic energy with wavelengths short enough to be useful for navigation purposes cannot penetrate the conductive seawater, and dead reckoning with inertial guidance systems accumulates too much error over the duration of a CSEM survey.

Acoustic navigation methods

Acoustic navigation systems are available in several different flavors (see below), but all rely on an interrogation/transponder system, whereby a transponder in the seawater listens for a burst of sound at a particular frequency and immediately replies with a similar burst of sound upon hearing this. The interrogation system, which generates an outgoing sound pulse and listens for the transponder's reply, measures the two-way travel time (TWTT) between the outgoing pulse and the reply. Sound speed in seawater is about 1,500 m/s, so the effective TWTT velocity is about 750 m/s.

Long base line (LBL) acoustic systems rely on triangulating a target location using TWTT data obtained from several widely spaced positions. Operational frequencies are in the range of 7 to 16 kHz, centered on 12 kHz, which offer a compromise between time resolution and losses during travel through water (LBL equipment is capable of working up to ranges of 10 km). In order to discriminate frequency to about 0.25 kHz resolution, bursts of sound (pings) about 10 ms long are used, and travel time discrimination is usually accurate to about one millisecond, providing one meter resolution for a single ping. Estimates of acoustic travel times could be improved to 5 microseconds with the use of specialized transponders (e.g., Spiess et al. 1998).

To navigate OBEM receivers equipped with a LBL transponder, a survey vessel can range on the OBEM from at least three different locations so that the OBEM location can then be triangulated. In practice the vessel ranges repeatedly on the OBEM while driving over the deployed position in a sensible survey pattern (e.g., two crossing lines over the instrument). The collection of TWTT data and GPS recordings of the ship's position are inverted using a layered model of the measured sound velocity profile, which accounts for the refraction and bending of the acoustic rays, yielding OBEM positions accurate to around one meter depending on water depth. Research vessels normally have 12 kHz transducer arrays permanently mounted on the vessel's hull that can be used in conjunction with the ship's GPS antenna for LBL navigation, after accounting for any heading dependent offsets between the GPS antenna and the acoustic transducer. Russell et al. (2019) presents a new LBL navigation code and demonstrates about 4 m position accuracy for seafloor seismometers deployed in 5000 m water depths. With even more careful application and long data stacking, LBL methods can be used to obtain the centimeter level precision required for studying the tectonic motions of the deep ocean seafloor (e.g., Spiess et al. 1998; Gagnon et al. 2005).

Some of the earliest marine CSEM surveys relied on seafloor based LBL navigation systems to determine the transmitter location (Evans et al. 1991; MacGregor et al. 1998, 2001). An array of LBL transponders was moored about 200 m above the seafloor, spaced about every 5 km along both sides of the intended tow line, and navigated after deployment in the same manner as done for OBEM receivers. The CSEM transmitter contained a relay transponder on the deep-tow package that was triggered by the replies from the moored transponders when the ship ranged on them, with the ship monitoring the replies from both the relay and the transponders. Thus the ship–transponder–relay–ship round-trip time was measured, along with the ship–transponder TWTT. By also measuring the direct range to the relay transponder on the transmitter, the relay–transponder distance could be recovered and was used to triangulate the transmitter position. Note that since the moored transponders are navigated prior to the CSEM survey, the transmitter navigation did not depend directly on the ship's position during the CSEM tow.

Short baseline (SBL, also ultra short baseline or USBL and super short baseline or SSBL) acoustic systems use higher operating frequencies (around 30 kHz) than LBL acoustics and more closely spaced transceivers. For SBL systems the transceivers may be spaced at different locations on the ship's hull in order to achieve triangulation without

requiring the vessel to move position. For USBL systems, the angle of incoming acoustic energy is estimated from measurement of phase differences across an array of receiver transducers mounted on a single transceiver head. The return angle is supplemented by the TWTT to provide a target location from a single interrogation pulse. The pitch, roll, and heading of the transceiver head needs to be monitored continuously using a motion reference unit (MRU) in order to convert the incoming angle to a vector in space, and the system needs to be regularly calibrated by sailing a pattern over an USBL transponder deployed on the seafloor. Such systems have advertised accuracies of about 0.25% in range and about 0.25° in angle. Under ideal operating conditions, one might thus expect range errors of no worse than 8 m and cross-range errors of no worse than 13 m for a position estimate from a single vessel location. In practice these figures are probably optimistic. For example, in our experience temporary installations of portable USBL systems tend not to perform as well as permanently installed and calibrated systems. Of course, for OBEM receiver navigation an USBL system can be used in the same mode as an LBL system by driving a pattern with the survey vessel, to obtain similar accuracies.

Currently, the standard approach to determining the location of a deep-towed CSEM transmitter and the vector of its dipole antenna is to mount an USBL transponder onto the transmitter package and also at one or more locations along the antenna, and range on these from the vessel during the survey tows. As we mention above, ideally one might expect range errors of order 10 m using such a system, but up to 50 m inaccuracies have been anecdotally reported for CSEM transmitter positions. This could be associated with errors in calibrating the USBL system and in the MRU operation during ship's motion. USBL systems are mainly limited to water depths on the continental margins since higher frequency USBL pings have limited ranges due to losses, and the angle uncertainty results in proportionally larger position errors in deeper waters.

The limited operational aperture (angle) of the ship-mounted USBL transceiver head can be a problem for packages with significant lay-back from the ship during towing, or with long transmitter antennas and receiver arrays towed behind the transmitter. In these cases the angle from horizontal between the ship and sub-sea transponders can become small and outside the field of view of the transceiver. One solution to recovering the antenna or array geometry is to mount an USBL transceiver on the deep-towed transmitter along with a deep-tow MRU, both suitably packaged in pressure housings, so that ranges and angles from the transmitter to transponders positioned on the antenna/array can be obtained. This approach is technically challenging and expensive, but has been used in the commercial application of CSEM methods.

Seafloor based LBL navigation offers the possibility for accurate positioning in all water depths, but is generally considered too tedious for modern CSEM surveys since the installation, surveying, and recovery of a seafloor transponder array requires significantly more time than is necessary for the CSEM transmitter deep-tows. Additionally, for extensive 3D survey grids with 100's of line kilometers of CSEM towing, prohibitively large numbers of LBL transponders would be needed.

In this work we describe a simple modification to the traditional LBL approach that allows it to overcome these limitations, so that the accuracy of LBL navigation can be obtained with a system that has a mobility and efficiency similar to the USBL method. This is accomplished by mounting the LBL ranging instrument on the deep-tow package (rather than the vessel) and surface towing an array of two or more GPS equipped transponders behind the vessel—an approach referred to as inverted long baseline (ILBL) navigation (Fig. 1). Note that unlike an USBL transceiver mounted on the deep-tow, the system is omni-directional and does not require an MRU.

Navigation accuracy requirements

Before describing the details of the ILBL system, we present a model study that demonstrates the level of navigation accuracy needed for a typical CSEM survey. Fig. 2a shows some example CSEM responses as a function of range (transmitter–receiver distance) for a simple model representing porous sediments with a 50 m thick target layer of variable resistivity located 1 km beneath the seafloor. Model responses for target layer resistivities of 1, 2, 4 and 8 ohm-m were generated at 0.25 Hz for a horizontal electric dipole transmitter 50 m above the seabed using an open-source 1D modeling code (Key 2009). The response anomaly (i.e., the relative difference) in the CSEM responses for the various target layer resistivities are shown in Fig. 2b, where the response of the model with a 1 ohm-m target layer is used for the normalization. All three models contain anomalies that exceed 1% at 2–10 km range. Since real survey data have been shown to exhibit data repeatability to within a few percent (Myer et al. 2012), we will use 1% error in the CSEM response as an equivalent bound on the accuracy required for the navigated transmitter and receiver positions.

Next we examine how errors in the position of the transmitter can affect the ability to reproduce survey data. We first consider horizontal position errors, which are decomposed into inline and crossline error components, where inline is the direction pointing along the line from the source to the receiver. Fig. 2c–d show the relative difference in CSEM responses computed for inline and crossline perturbations of the transmitter position by adding 4 to 128 m offset. Because

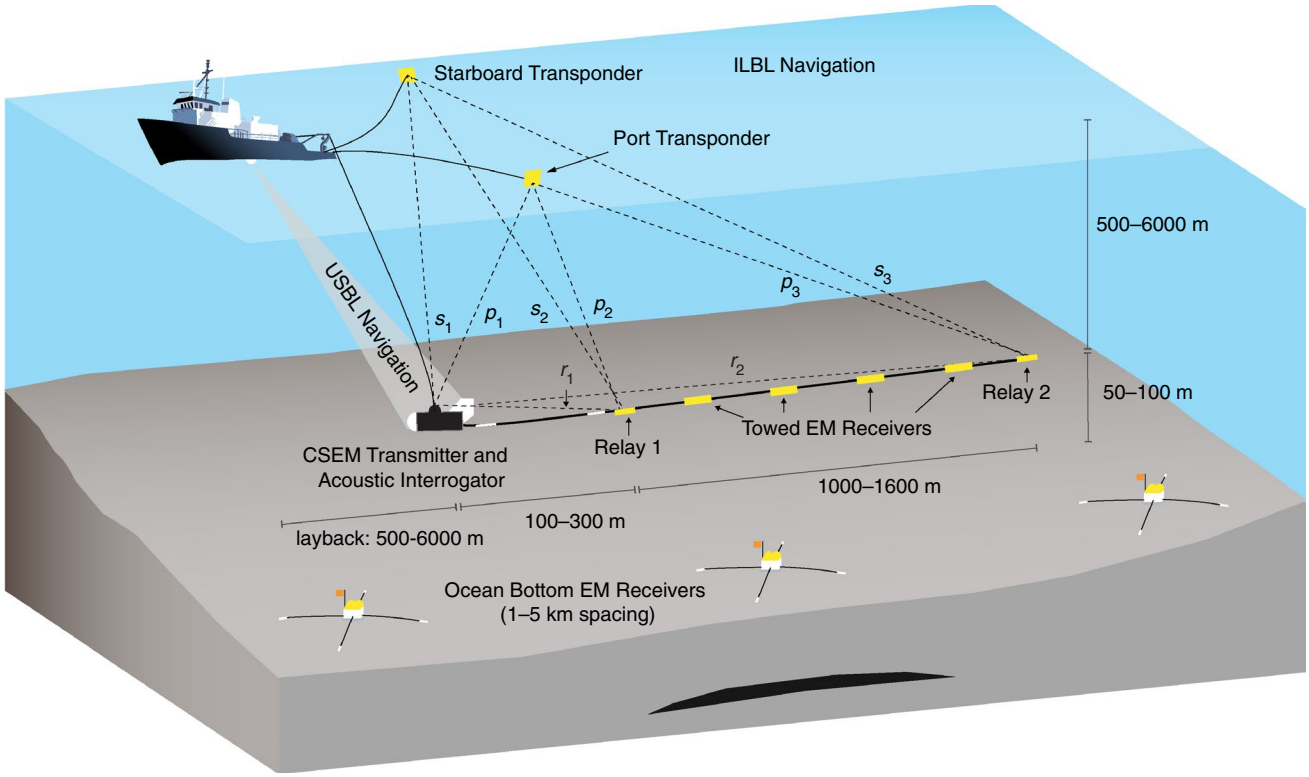

Fig. 1 Conceptual diagram of an inverted long-baseline acoustic navigation system for navigating a deep-towed CSEM transmitter and antenna array. Two transponders are surface-towed on paravanes behind the ship while their GPS positions are broadcast to the ship over radio modems. Acoustic travel times (dashed lines) are measured by ranging from the acoustic interrogator on the CSEM transmitter to two surface-towed transponders (paths p_1 and s_1) and to relay transponders located at the end of the antenna and the towed receiver array (paths r_1 and r_2). Three part relay paths are obtained by measuring replies from the surface towed transponders when triggered by the relay transponder replies (paths r_1-p_2-p_1, r_1-s_2-s_1, r_2-p_3-p_1 and r_2-s_3-s_1). Conventional USBL navigation relying on a single range and angle measurement is shown as the shaded white region emanating from a hull mounted transceiver on the ship

the source field decays rapidly with range, the inline perturbations result in significantly larger response errors than crossline perturbations. From this study we conclude that in order to obtain data accurate to 1% at ranges greater than a kilometer (where the data are most sensitive to the target structure), the inline position must be known to within 4 m while the crossline position has a much less stringent requirement of around 64 m. For higher frequency transmissions where the EM fields decay more rapidly due to increased inductive attenuation, more accurate navigation is required to meet the 1% error level. At offsets less than 1 km where data may be collected for mapping targets located at only tens to hundreds of meters depth, significantly more accurate navigation is needed (Constable et al. 2016).

Finally, in Fig. 2e-f we consider the effects of errors in the transmitter antenna heading and dip angles. For the idealized case of inline data where the transmitters and receivers are located precisely on the survey line, the data amplitudes exhibit a cosine dependence on the antenna heading that is range independent, so that the heading angle only needs to be known to about 8° to obtain 1% accuracy. For commercial surveys, the receiver drop locations are given about a 50 m tolerance for deviations from the planned locations and the transmitter can also drift off the survey line due to bottom currents. Hence we have included a known 50 m crossline offset between the transmitters and receivers in the study shown in Fig. 2e, which acts to amplify the heading angle errors at short offsets due to the larger relative azimuth between the transmitter and receiver. In this case, the heading angle would need to be known to about 4 or 5° to obtain 1% accuracy at offsets greater than 1 km.

A dipping transmitter antenna results in the more complex behavior shown in Fig. 2f. Consequently, a 1° dip accuracy is required to obtain 1% data accuracy; this is particularly important since errors in the dip angle produce changes in the modeled CSEM responses at 2–8 km offset that resemble the anomalies due to variable target layer resistivities (compare Fig. 2f with Fig. 2b).

To measure the heading angle of the transmitter antenna, transponders are placed at each end of the antenna. For a given transponder position uncertainty, the resulting heading uncertainty scales in inverse proportion

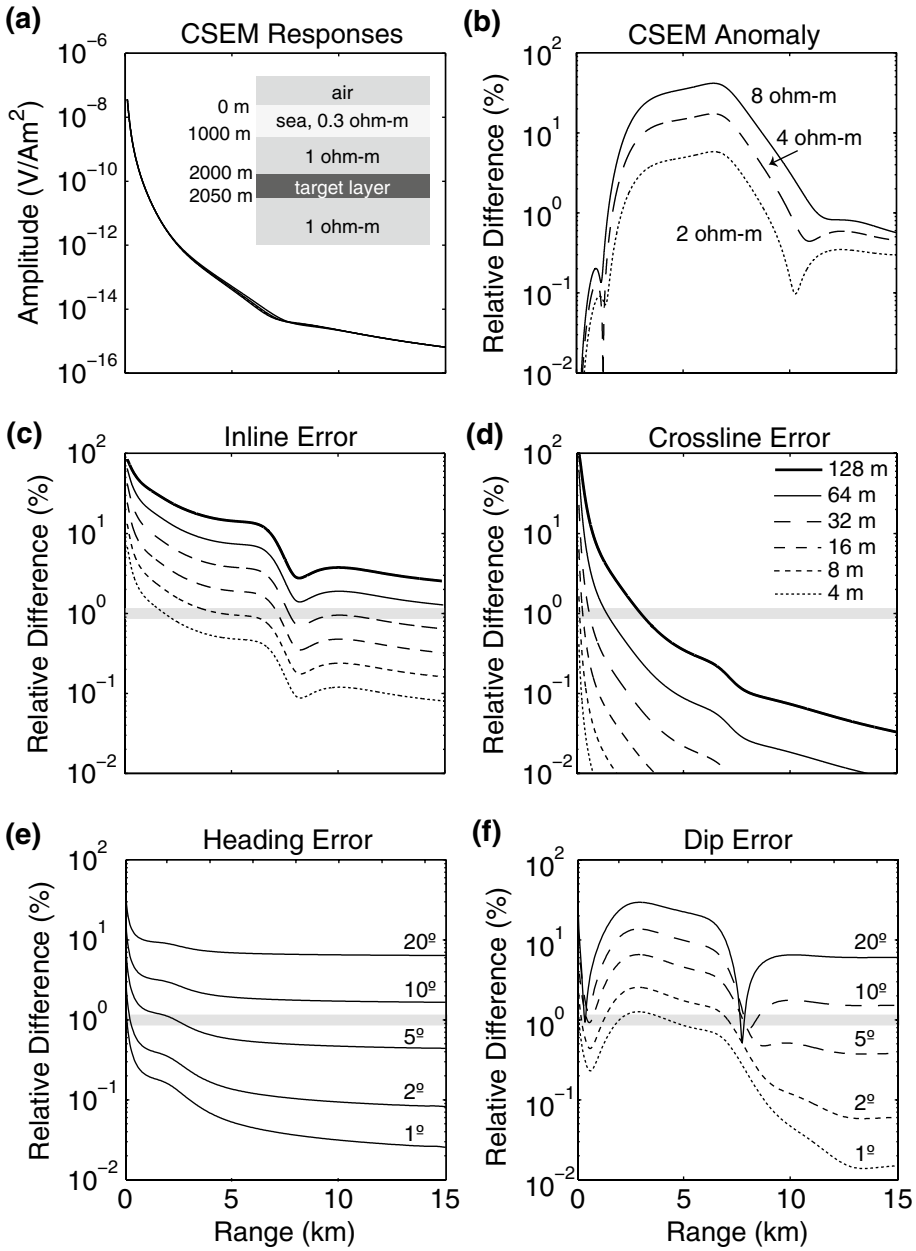

Fig. 2 Model study of the effect of transmitter navigation errors on CSEM responses. **a** The inline electric field amplitude for the 1D model shown in the inset. **b** CSEM response anomalies generated by three different values of target layer resistivity. The effects of inline (**c**) and crossline (**d**) transmitter position errors of 4 to 128 m. The effect of errors in the transmitter heading (**e**) and dip (**f**) angles. The heading error study included a known 50 m crossline offset between the transmitter and receivers

Table 1 Antenna endpoint position uncertainty (m) required to obtain heading and dip estimates accurate to 1°, 5° and 8° for various antenna lengths

Antenna Length (m)	1°	5°	8°
10	0.17	0.87	1.4
100	1.7	8.7	14
1000	17	87	140

to the length of the antenna. Table 1 shows the corresponding position uncertainties needed to obtain angle estimates accurate to 1°, 5° and 8° for dipole lengths of 10, 100 and 1000 m. These values also apply to the depth uncertainty required to obtain accurate antenna dip measurements. As described below, modern pressure (depth) sensors are accurate to better than 1 m and so 1° dip accuracy can be obtained for the typical 100–300 m dipoles used for deep CSEM exploration, whereas the much shorter (10-50 m) antennas used for shallow mapping require more accurate pressure measurements.

Accurate interpretation of standard CSEM data also requires precise knowledge of the positions and orientations of the seafloor EM receivers. We refer to Myer et al. (2012) for a comprehensive error analysis that looks at the compounding influence of errors in both the transmitter and receiver positions and orientations in the context of assigning uncertainties to real survey data.

Description of system

Figure 1 shows a schematic of the configuration of the ILBL navigation system and the deep-towed CSEM array. Below we review the development of the ILBL system and its components.

We built a second-generation CSEM transmitter system to replace the one described in Constable and Cox (1996) and which we have named SUESI (Scripps Undersea Electromagnetic Source Instrument). It is designed to operate on standard 17 mm coaxial oceanographic deep-tow cable and is capable of up to 500 A transmission on antennas 50–300 m long. Constable (2013) gives a detailed description of this new system and relevant survey applications are described in Weitemeyer et al. (2011), Myer et al. (2012), Key et al. (2012), and Constable et al. (2016).

The new system uses a frequency-shift keyed (FSK) telemetry to provide bidirectional data transfer along the tow cable at 9600 baud, which allows us to monitor various environmental parameters during operation. Besides component temperatures and output current, these include the navigational parameters of depth (from a Valeport Midas conductivity–temperature–depth–sound velocity probe), and altitude (from a Kongsberg-Simrad 1007 series altimeter). Depth at the end of the transmission antenna is measured with a Digiquartz series 8000 pressure transducer that uses the pressure-dependent resonance of a quartz crystal, with a depth range of 0–7000 m and a quoted accuracy of < 0.7 m (similar to the sensor in the Valeport instrument). In our initial implementation, depth at the tail end of the antenna was only recorded by a serial data logger for viewing after the survey, but recently we updated the system so that it is now telemetered up to the ship along with the other real-time environmental data (see Constable et al. (2016) for details).

Our first step in designing the ILBL system was to repackage a Benthos DS-7000 acoustic transceiver unit into a pressure case that could be mounted on the SUESI. This device has a remote mode of operation in which it can be controlled by a computer over an RS-232 serial interface. With a simple set of commands the computer can choose the transmit and reply frequencies, the gains, any hold-off period to ignore replies after transmission, and trigger an interrogation ping. The TWTT from any replies are then sent to the host computer over the serial link, along with a time stamp from the internal clock. The DS-7000 has 4 receive channels, so replies at up to 4 different frequencies can be simultaneously recorded from each outgoing ping. The only modifications we needed to make besides the physical repackaging were to provide external 24 V power from the SUESI power bus, provide a simple circuit to reset the unit after power has been applied, and make connections to an external 12 kHz transducer head (an ITC model 3013) and the I/O serial lines. The power and serial lines are connected to SUESI over a standard 4-conductor underwater cable and connectors, and the transducer head by a similar 2-conductor cable. Fig. 3(a) shows the deep-towed SUESI transmitter and the relevant ILBL components.

In our first attempt at using the DS-7000 for SUESI navigation we tried to range on the deployed array of OBEM receivers (rather than surface towed transponders), each of which was equipped with an LBL transponder listening at various frequencies in half-kilohertz steps between 9.5 and 14.5 kHz (except 12.0 kHz, the reply frequency, and 12.5 kHz, which had been problematic in the past on account of being close to 12.0 kHz). Apart from taking advantage of an extensive array of LBL transponders, the source–receiver distance is exactly the parameter needed in CSEM analysis,

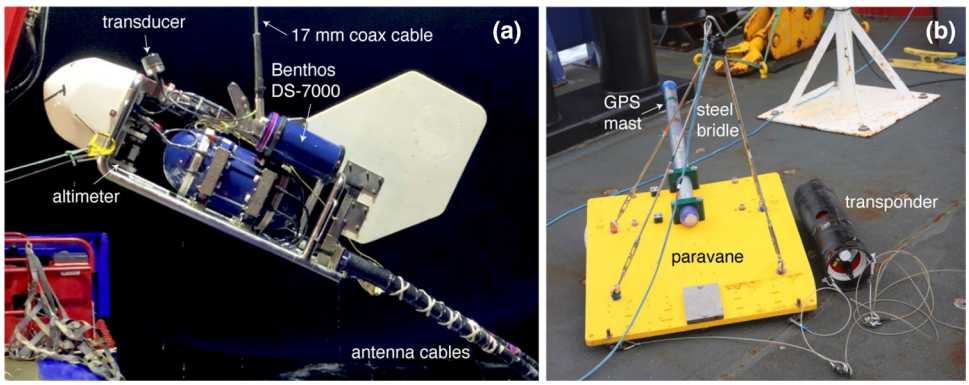

Fig. 3 **a** Photograph of the deep-towed SUESI vehicle and ILBL system components. Labels denote the pressure case housing the Benthos DS-7000 acoustic transceiver unit and its forward and upward pointing acoustic transducer, the altimeter, deep-tow cable and CSEM antenna cables. The Valeport pressure sensor (not shown) is located on the far side of the vehicle. **b** Photograph showing the paravane setup, including the steel bridle, GPS mast and hanging transponder

so it made some sense to try to measure it directly. However, it is well known that the positive sound velocity gradient near the seafloor is such that acoustic rays bend upward, making it difficult to range on seafloor instruments from near the seafloor; we were hoping that the 100 m tow height of the transmitter would provide reasonable acoustic ranges. Indeed, when we tried this we found that the OBEM receivers preferentially replied on the outgoing ping after it had bounced off the sea surface, rather than on the direct arrival. This led to the idea of placing the transponders on the sea surface, rather than the seafloor.

We thus constructed two paravanes from 2 cm thick polyethylene sheets that were approximately 60 cm square. One of our standard LBL acoustic transponders was mounted near the bottom of the sheet, and flotation was provided by a 15 cm diameter PVC pipe, 60 cm long and with end caps cemented on. We used a 4-point towing bridle made from stainless steel rods with turnbuckles for minor adjustment, finding appropriate lengths by trial and error (earlier efforts using rope bridles were prone to collapse during turns). This rigid bridle has proved to be unconditionally stable; for example on the Scarborough cruise described below, we deployed it without mishap for a total of 300 km of transmitter tow which included 16 turns.

Initially, having the transponders mounted directly to the base of the paravanes worked well for hearing pings from the transmitter when deep-towing up to 1 km depth in calm seas, but in later surveys where deep-towing extended to 5 km depths, the transmitter pings were too weak to be heard above wave noise. However, simply hanging the transponders 1-2 m below the paravanes using steel cables provided enough isolation from the surface noise that pings from the transmitter could be reliably heard, even when towing at 5 km depth.

To monitor the position of the paravanes during operations, we use a GPS receiver and 900 MHz radio modem, installed in a vertical PVC tube and mounted onto the flotation. Under control of a PIC microcontroller, GPS time and position fixes are broadcast to the research vessel over the radio link every few seconds. The PVC mast also contains flashing LED lights that turn on at night, and contains enough batteries to operate for 6 days. Fig. 3b shows the paravane configuration; for want of a name, we call these assemblies 'Barracudas'.

Table 2 lists the acoustic interrogation listen and reply frequencies. Our initial setup mimicked the 12.0 kHz replies of our OBEM transponders, but we noticed that this is an exact (30th) harmonic of the 400 Hz power we use for the transmitter, and the various components and transformers produce enough 12.0 kHz acoustic noise to degrade the ping detection on the Benthos DS-7000 at this frequency. We originally carried out sequential interrogation of the port and starboard Barracudas, but during the elapsed time between interrogations the system has moved slightly, which introduced a measurable error after we analyzed the data. We thus modified the transponders to listen at 12.5 kHz and reply at two different frequencies, 8.5 and 9.0 kHz, exploiting the fact that we had 4 channels available to listen on the DS-7000.

Table 2 The acoustic transponder interrogation listen and reply frequencies used for the ILBL system

	Listen (kHz)	Reply (kHz)
Port	12.5	9.0
Starboard	12.5	8.5
Relay 1	15.5	12.5
Relay 2	8.0	12.5

Finally, we mounted a relay transponder on the tail buoy attached to the end of the transmitter antenna (Relay 1 shown in Fig. 1) in order to obtain relays to the surface transponders that allow us to measure the antenna heading angle. The relay listens at 15.5 kHz and replies at 12.5 kHz, thus the Benthos system on SUESI measures the direct reply from the relay transponder as well as the relays through the surface transponders (paths r_1-p_2-p_1 and r_1-s_2-s_1 in Fig. 1).

In the most recent configuration of the system, the transmitter antenna has been augmented with up to a 1.6 km long array of four to six evenly spaced towed EM receivers (referred to as 'Vulcans') that allow for continuous recording of short offset EM fields that are useful for mapping shallow targets such as gas hydrates (Kannberg and Constable 2020; Constable et al. 2016). A tail buoy at the distal end of this receiver array contains an additional relay transponder (Relay 2 shown in Fig. 1) and a pressure sensor which are used for determining the heading and dip angles of the array. In this configuration, the Benthos DS-7000 is set to ping sequentially on 12.5, 15.5 and 8.0 kHz and listen to 8.5, 9.0 and 12.5 kHz, thus measuring all eight rays paths shown in Fig. 1.

Position estimation

Given the GPS determined locations of the paravane transponders, the TWTTs between the transmitter and transponders, and the transmitter's depth, the lateral position of the transmitter can be estimated by simple geometric reduction when a uniform seawater velocity is assumed. In this case, the TWTT data can be converted to horizontal range rings about each paravane that intersect at two locations. The intersection corresponding to the correct transmitter location is easily resolved based on geometric arguments (i.e., the intersection furthest behind the vessel, or that best matches the predicted horizontal range given the amount of deep-tow wire out). The

uncertainty of the transmitter position can be estimated by propagating the uncertainties of the TWTTs and the paravane locations into horizontal range uncertainties.

While this simplified approach may be sufficient for short range applications where the velocity can be assumed to be uniform, a more accurate estimate can be obtained by accounting for the refraction of the acoustic rays due to the large velocity gradient in the upper part of the ocean. For nearly vertical angles of incidence an equivalent depth averaged velocity can be used; however, the ILBL acoustic ray paths are necessarily inclined to the velocity gradient given the paravane aperture as well as the significant layback of the transmitter, and hence experience a variable amount of refraction depending on the particular survey geometry and transmitter tow depth. As an example of the ray angles, consider a deep-tow transmitter at 1000 m depth. The deep-tow wire typically maintains an angle of about 45° from horizontal due to its drag, placing the transmitter 1000 m behind the ship. With paravanes positioned 400 m behind the ship, the transmitter layback is 600 m. A 1000 m long towed receiver array attached to the transmitter has a 1600 m layback. Including a 150 m crossline offset for each paravane, these laybacks result in a 58° angle from the sea surface for paths s_1 and p_1 and a 32° angle for paths s_3 and p_3.

Our position estimation procedure accounts for refraction by ray-tracing the acoustic paths through a layered velocity model (e.g., Shearer 2009), where the velocity profile is obtained by direct measurement using data from the Valeport sensor mounted on SUESI as it is lowered towards the seafloor at the start of a survey line and later when it is hauled back to the sea surface.

The ray-tracing algorithm acts as the forward modeling operator in a Levenberg-Marquardt non-linear parameter estimation scheme (e.g., Aster et al. 2019) that inverts the TWTT data for the transmitter location. We have found that typically only a few iterations are required to fit the TWTT data when a sensible starting guess is used for the transmitter position. This could be a dead reckoning estimate projected from previously determined positions, but in our experience simply using the position from the previous solution works well as a starting guess. For the initial position estimate, a rough guess using a location slightly aft of the paravanes has been found to work well. Since only two TWTT data are used to estimate the two horizontal position parameters, the Levenberg-Marquardt scheme can usually fit the TWTT data to well below their assigned uncertainty of 1 ms.

Position uncertainty

The uncertainty in the estimated transmitter position depends not only on the uncertainties in the TWTT data and the paravane transponder locations, but also on the normalized

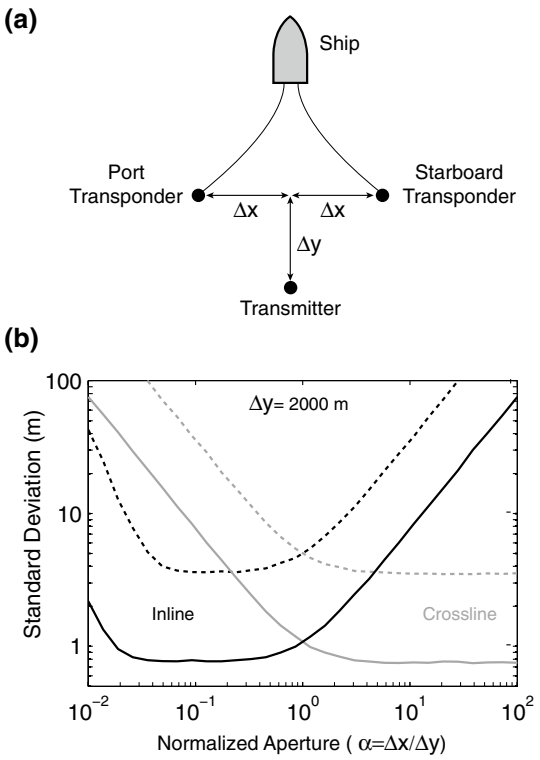

Fig. 4 **a** Plan view of the ILBL survey geometry showing the relative horizontal offsets between the surface towed transponders and the deep-towed CSEM transmitter. **b** Results of Monte Carlo simulations for the inline (y) and crossline (x) transmitter position uncertainty are shown as a function of normalized aperture for a 2000 m layback (Δy) assuming 1 m (solid) and 5 m (dashed) standard deviations for the transponder locations and 0.5 ms Gaussian noise for the TWTT data

aperture of the transponder array, as shown in Fig. 4. Here we define the normalized aperture as $\alpha = \Delta x/\Delta y$, where Δx is the crossline distance of each transponder from the towpath and Δy is the layback of the transmitter from the transponders.

It is straightforward to demonstrate how the normalized aperture impacts the uncertainty in the ILBL estimates by conducting a Monte Carlo error simulation. We generated 4000 synthetic transponder range samples for a fixed transmitter position with 2000 m layback and a given α. The transponders' inline and crossline positions were randomly perturbed by 1 or 5 m Gaussian noise and the TWTT data perturbed by 0.5 ms Gaussian noise. For each of the 4000 samples, we estimated the transmitter position using the same scheme as used for the real data examples shown later in this work. From this we can determine the uncertainty in the transmitter position by taking the standard deviation of the 4000 positions. We ran this simulation to estimate the position uncertainties associated with α spanning logarithmically from 0.01 to 100, with the results shown in Fig. 4b.

For 5 m transponder noise the position uncertainty is as low as 4 m while the 1 m transponder noise gives position

uncertainty as low as 0.8 m. However, the relative size of the inline and crossline uncertainties is highly dependent on α. As the α becomes much greater than unity, the inline position uncertainty grows linearly with α while the crossline uncertainty asymptotes to a minimum value; conversely the crossline uncertainty grows as α^{-1} when α is much less than unity.

If one desires to distribute the uncertainty equally between the inline and crossline positions, then clearly α close to unity is optimal; however, a 20-30% reduction in the uncertainty is obtained when α is within a factor of ten above or below unity, depending on the position component. Since our earlier model study showed that errors in the inline position are significantly more important than the crossline position, it appears that $\alpha \approx 0.1$ would be ideal for minimizing the inline uncertainty; while this results in the crossline uncertainty being about 10 times larger, the model study in Fig. 2d shows that this would have negligible impact on the CSEM responses for either the 1 or 5 m transponder uncertainties. From a practical viewpoint, $\alpha \approx 0.1$ is also desirable since the transponders don't need to be towed as far laterally away from the ship, which could be impractical for a paravane system. For example, with a 2000 m layback, $\alpha = 0.1$ corresponds to the transponders being positioned only 200 m to the port and starboard of the tow path whereas 2000 m lateral offset would be needed to have a unity aperture ($\alpha = 1$).

The 5 m transponder position uncertainty corresponds to that of the low-power GPS units mounted on the Barracuda paravanes; thus we can expect the ILBL position uncertainties to be as low as about 4 m when the layback is around 2000 m. If more accurate positioning of the tow vehicle is desired, then more accurate GPS receivers using a differential system should be utilized.

Survey examples

Here we present three example applications of the ILBL system. For these surveys, the paravanes were deployed on fixed lines to give crossline Δx values from 100 to 150 m. Since the transmitter layback increases with its depth due to the the typical 45° angle of the deep-tow wire caused by drag, the normalized aperture therefore decreases with transmitter depth. TWTT data were acquired about every 10 s and we linearly interpolated the paravane GPS positions to the time of each TWTT pair. Prior to solving for position, we trimmed obvious outliers from the TWTT data and removed the occasional late arrival occurring from reflections off the seafloor. As expected from the uncertainty analysis shown above, the resulting navigation solutions for each TWTT pair display scatter due to random noise in the TWTT data as well noise in the paravane positions. To further improve the navigation, we applied a robust moving average smoothing filter independently to the inline and crossline positions. This gives smoothed positions that have point to point velocity values that agree well with the ship's velocity. As a robust measure of the uncertainty in the solutions, we use the estimator $\hat{\sigma} = 1.4826$ MAD, where MAD is the median absolute deviation of the individual position estimates x_i from the robustly smoothed positions $\bar{x}_i$, computed over a set of samples $i = 1, ..., N$:

$$\text{MAD} = \text{median}(|x_i - \bar{x}_i|). \quad (1)$$

The factor 1.4826 accounts for the theoretical difference between the standard deviation of normally distributed data and the MAD.

Middle America Trench

Data from the Middle American Trench offshore Nicaragua demonstrate the performance of the system at 1 to 5 km tow depths. Acquired in 2010, the CSEM survey targeted conductivity variations from faulting, hydration and anisotropy associated with widespread normal faults induced by the bending moment of the incoming Cocos Plate prior to its subduction (Fig. 5). The resulting CSEM images of seafloor conductivity are presented and interpreted in Key et al. (2012); Naif et al. (2015, 2016). The full data set includes over 300 km of deep tows and here we only present results from the main 150 km long profile, which was spliced together from two different deployments of the system. The navigation results are summarized in Figs. 6–8.

Most of the profile has large 3 to 5 km tow depths with normalized apertures of about 0.02 to 0.04, but the aperture

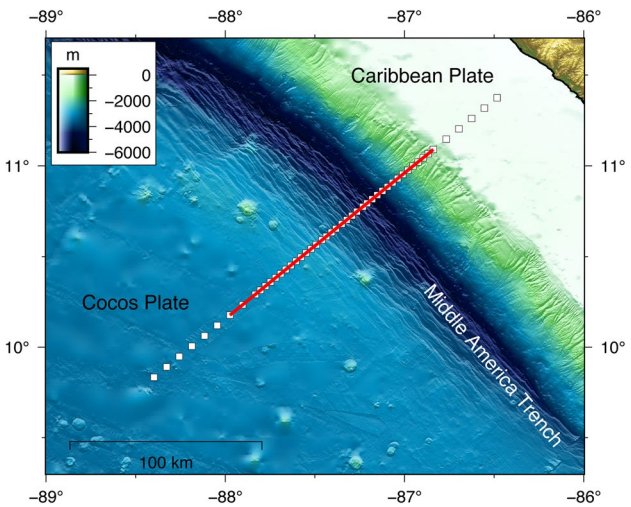

Fig. 5 Map showing the CSEM survey of the Middle America Trench offshore Nicaragua with topography (shaded colors), OBEM receivers (white squares) and the ship track for the CSEM deep tow survey (red line)

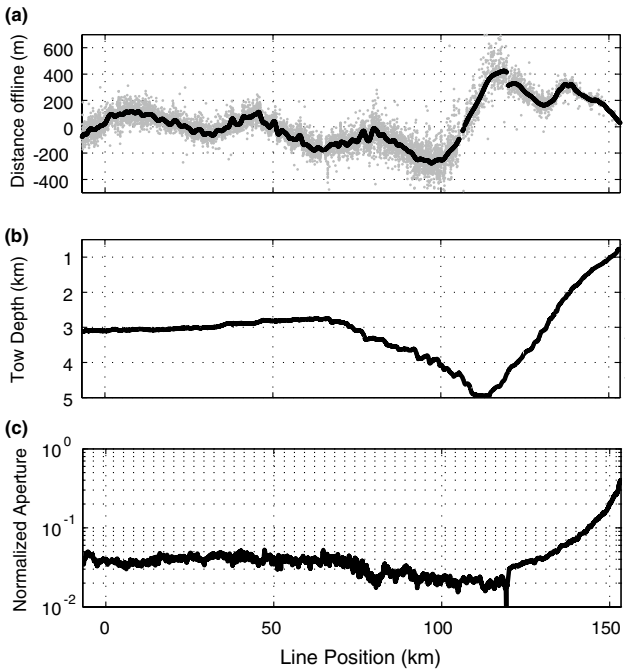

Fig. 6 Example of ILBL navigation for a deep tow CSEM survey of the Middle America Trench offshore Nicaragua. **a** Offline distance of the navigated transmitter position relative to the planned survey line shown for raw solutions from individual pairs of TWTT data (grey dots) and smoothed positions (black dots) after applying a 300 point robust moving average. **b** Transmitter tow depth along the profile. **c** Normalized aperture α as a function of position along the profile. Note that this profile was acquired using two separate tows and the navigation data were spliced together around 120 km position

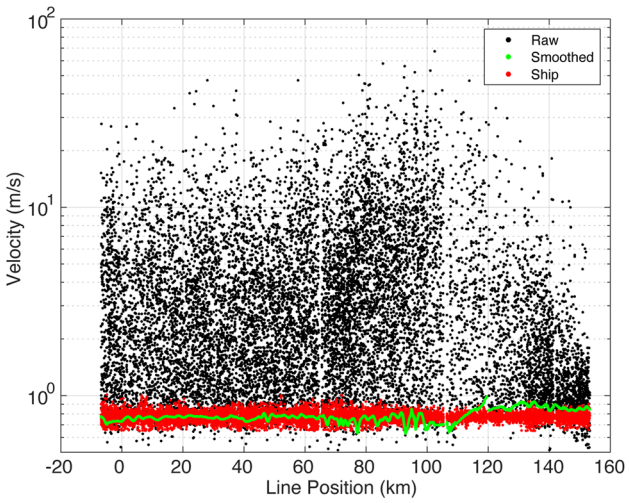

Fig. 7 Middle America Trench ILBL navigation results showing the velocity computed from point to point differencing of the raw navigation solutions (black) and the robustly smoothed solutions (green), along with the ship velocity (red). The large scatter in the raw solutions is predominantly caused by point-to-point scatter in the raw crossline position data (see Fig. 8a). Although the ship velocity is nearly constant, the smoothed deep-tow velocity shows a small reduction in velocity when the deep-tow cable was paid out as the transmitter was lowered down into the trench near 100 km position, and a small increase in deep-tow velocity as the cable was hauled in while towing up the continental slope at 120 to 150 km position

increases up to 0.4 at the shallower depths on the continental slope near the profile's end. As expected, the scatter in the raw solutions is considerable and clearly correlates with increasing tow depth and decreasing normalized aperture (Fig. 6), with the largest scatter for the deepest data near 100 km position and the smallest scatter for the shallowest data near 150 km position.

We found that a 300 point robust moving average smoothing filter works well for reducing the position scatter. As confirmation, we computed the apparent horizontal velocity of the transmitter by dividing the point to point differences in position by the corresponding time difference. Fig. 7 shows the resulting estimated velocities for the raw and smoothed navigation solutions. Velocities from the raw data have considerable scatter due to the large random noise in the crossline positions, whereas the smoothed positions agree remarkably well with the 0.7 m/s velocity of the ship, as they should given that the transmitter is attached to the ship by the deep-tow cable. Some small differences between the smoothed deep-tow velocity and the ship velocity can be explained by a small reduction in tow velocity while paying out the deep-tow cable as the transmitter was lowered down into the trench (near 100 km position) and a small increase in velocity as the cable was hauled in while towing up the continental slope (120 to 150 km position).

Histograms of the residual between the raw and smoothed positions provide an uncertainty measure for the raw solutions (Fig. 8). At transmitter positions around 62–67 km where the tow depth was around 3 km and the normalized aperture is 0.035, the inline spread is about 5 m while the crossline spread is about 37 m. At transmitter positions 147–152 km where the depth shallows to near 1 km and the normalized aperture increases to 0.35, the inline spread is about 6 m while the crossline spread significantly reduces to around 6 m. These deep and shallow results agree with the uncertainty study shown earlier, where for apertures below unity, the inline uncertainty is consistently small while the crossline uncertainty grows in proportion to the inverse of the aperture. The raw position uncertainty level is already below the navigation requirements determined from forward modeling earlier in this work, while the smoothed positions will have uncertainties about an order of magnitude smaller than this given the $\sqrt{N}$ reduction from averaging $N = 300$ points. Thus we can conclude that the ILBL system works well for navigating the CSEM transmitter at water depths up to at least 5 km. Importantly, the up to 400 m offline set of the transmitter while deep-towing across the trench is well-measured by the ILBL data and would otherwise corrupt the interpretation of the CSEM receiver data if navigation data

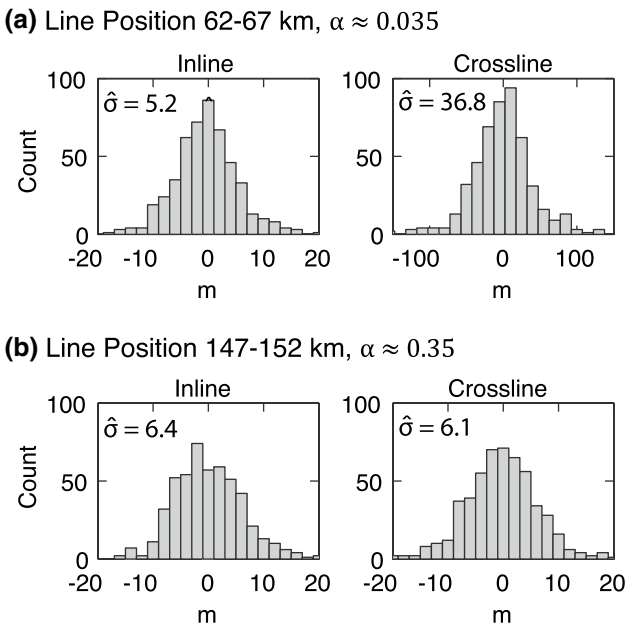

Fig. 8 Histograms computed from the residual differences between the raw navigation solutions for individual TWTT data pairs and the 300 point robust moving averages shown for inline and crossline positions for tow sections with depths of about 3 km (**a**) and 1 km (**b**). The corresponding robust measure of spread $\hat{\sigma}$ is inset in the upper left of each histogram

were unavailable and the transmitter was instead assumed to directly follow the ship track.

San Nicolas Basin

Our second example shows ILBL navigation not only for the transmitter position but also for the position of two relay transponders in a configuration similar to that shown in Fig. 1, with Relay 1 at 125 m from the transmitter and Relay 2 at 1088 m just beyond the fourth towed EM receiver. The 2013 CSEM survey of the San Nicolas Basin in the southern California continental borderlands (Fig. 9) was carried out as part of the development of a towed transmitter-receiver array for making continuous CSEM measurements sensitive to shallow methane gas and hydrates in the seafloor. For testing the ILBL system, we also made navigation measurements of the transmitter position using an independent USBL system installed on the survey vessel (a Sonardyne GyroUSBL 7000 system). Although the CSEM results from the San Nicolas Basin survey are unpublished, two-dimensional resistivity inversion images from using this system to survey the nearby Santa Cruz Basin are given in Kannberg and Constable (2020).

During the survey, direct TWTT data were collected between the transmitter and the relays (paths r_1 and r_2 in Fig. 1). Three way travel time data were recorded for Relay 1 on paths r_1-p_2-p_1 and r_1-s_2-s_1, which were then reduced to TWTT for paths p_2 and s_2 by subtracting off the travel times

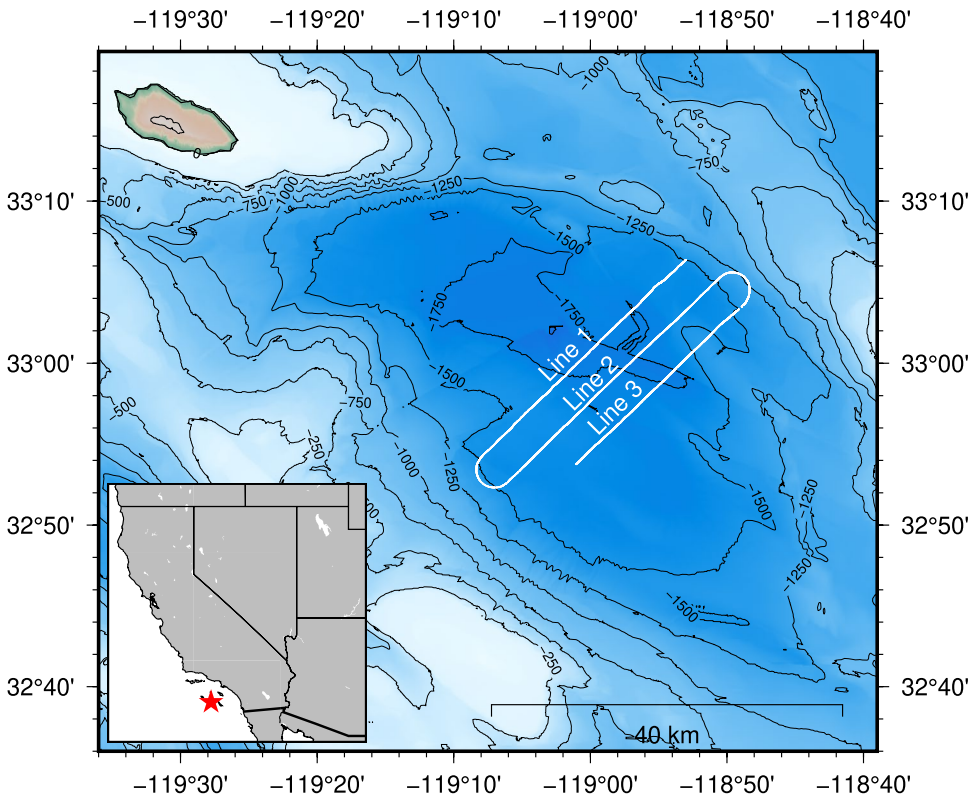

Fig. 9 Marine CSEM survey location at San Nicolas Basin in the southern California borderlands. White lines show the ship track while deep-towing the Vulcan EM transmitter-receiver array. Inset map shows the survey location (red star) offshore Southern California

for the direct paths p_1, s_1 and r_1. This allowed us to navigate Relay 1 independently of the transmitter position, and meant these travel time data could be inverted for position using the same processing code as used for the transmitter's travel time data. A similar method was used for navigating Relay 2.

Navigation results for survey Line 1 are summarized in Figs. 10 and 11, where an 80 point robust smoothing filter applied to the raw navigation solutions and only the smooth solutions are shown. We note that standard processing of USBL data includes a Kalman filtering scheme that performs as similar function to our robust smoothing filter. For this 26 km long profile in water depths of 1.5 to 1.7 km, the normalized aperture of the transmitter and Relay 1 are about 0.1 while Relay 2 is around 0.04. Both the ILBL and USBL solutions for the offline transmitter position agree broadly, with up to 100 m offset from the planned survey line. For most of the profile the ILBL and USBL solutions agree to better than 10 m offline position, but around 10 to 13 km position the solutions diverge by up to 40 m. The source of this disagreement is not clear; although not shown here, the inline positions for the ILBL and USBL systems agree to better than 10 m for most of the survey, yet at this location the disagreement in the inline solution grows to as large as 20 m. The Relay 1 offline position is generally close to the transmitter as expected given its short 125 m offset, whereas Relay 2 has offline positions up to 200 m from the profile, likely due to the influence of lateral water currents during the course of the tow.

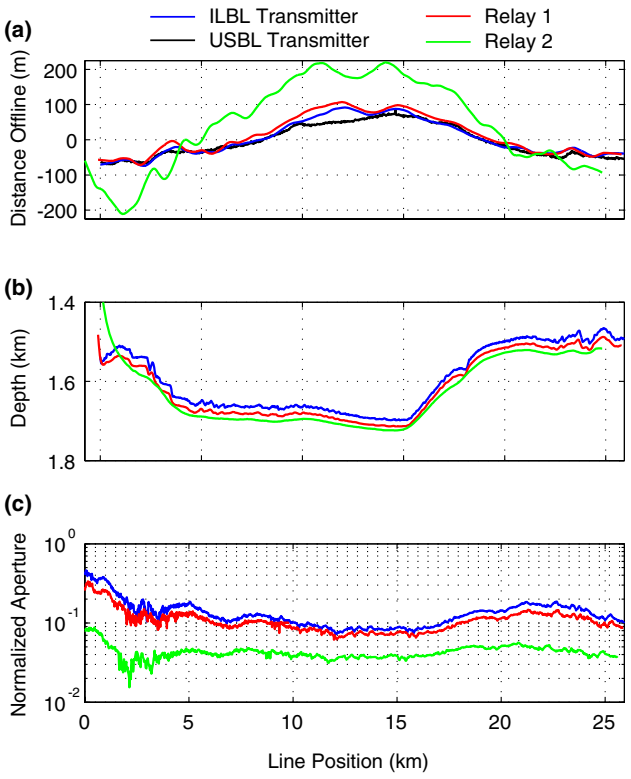

Fig. 10 San Nicolas Basin survey ILBL navigation results for Line 1. **a** ILBL solution for the offline position of the transmitter, Relay 1 and Relay 2 (blue, red and green lines, respectively) and the transmitter position determined using an independent USBL navigation system. **b** Depths of the transmitter, Relay 1 and Relay 2 during the deep-tow. **c** Normalized aperture α of the paravanes relative to the layback of the transmitter, Relay 1 and Relay 2 shown as a function of position along the profile

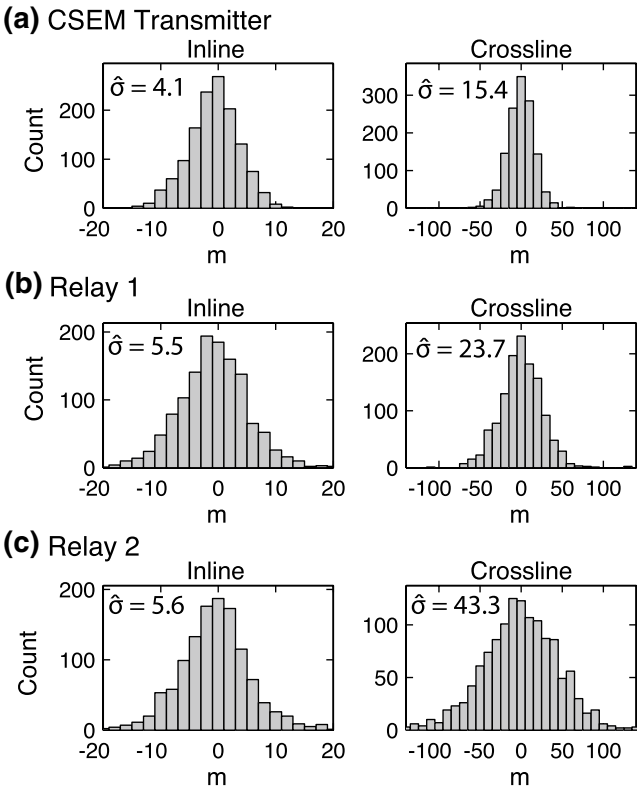

Fig. 11 San Nicolas Basin survey ILBL navigation results histograms computed from the residual differences between the raw solutions for individual TWTT data pairs and the 80 point robust moving averages shown for inline and crossline positions for the **a** CSEM transmitter, **b** Relay 1 and **c** Relay 2 on the combined transmitter-receiver array. The corresponding robust measure of spread $\hat{\sigma}$ is inset in the upper left of each histogram

Residual histograms (Fig. 11) show the raw inline positions for the transmitter, Relay 1 and Relay 2 have about the same inline uncertainty of about 5 m, whereas the crossline uncertainty increases to values of 15, 24 and 43 m, respectively. Since the crossline positions of the transmitter and Relay 1 are used to estimate the azimuth angle of the source antenna, these can be converted into azimuth uncertainty using standard linear propagation of uncertainty formulas. Omitting the details, we find an azimuth uncertainty of 13° for the raw solutions, whereas the $N = 80$ point average for the smooth positions yields an azimuth uncertainty of 1.5°, assuming a $\sqrt{N}$ uncertainty reduction.

Exmouth Plateau

Our final example is the 2009 survey of the Scarborough gas field on the Exmouth Plateau about 250 km offshore northwestern Australia, where CSEM data were collected to study how the method can be used as a hydrocarbon mapping tool (Myer et al. 2012, 2015). The month long survey acquired a total of 144 OBEM deployments and over 600 km of CSEM transmitter tows with sea bottom depths around 900-950 m. Here we examine the ILBL navigation for the second phase of the survey where CSEM deep-tows were carried out continuously for six and a half days on a grid of 12 intersecting profiles. Fig. 12 shows the positions of the Barracuda paravanes during this survey phase. The paravanes maintained a consistent separation with Δx having a mean value of 133 m and a standard deviation of 14 m. Despite the various tow line directions and the 11 turns with variable radii, the paravanes maintained a consistently stable geometry, illustrating the reliability of the ILBL navigation system. The only problem encountered was when the battery in the starboard paravane's radio died during the middle of this phase; the paravane was retrieved and swapped out with a new radio mast, interrupting only a short segment of the tow. Uncertainties computed for the raw ILBL navigated positions for each tow line are less than 4 m for the inline position and 8 m for the cross line position. Fig. 13 shows a perspective view of the navigated position and depth of the deep-tow transmitter, including the turn sections where the transmitter is raised high above the seafloor as a precautionary measure. Further details of the CSEM data and an aggregate uncertainty analysis accounting for uncertainties in the transmitter and receiver positions and orientations are given in Myer et al. (2012).

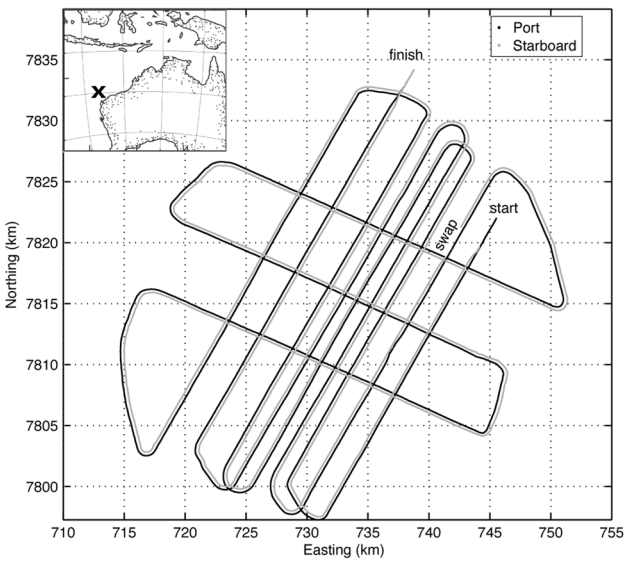

Fig. 12 ILBL navigation tracklines for the CSEM survey of the Scarborough gas field on the Exmouth Plateau about 250 km offshore northwestern Australia (Myer et al. 2012, 2015). Black and gray lines show the Barracuda paravane positions during Phase 2 of the month-long survey. The inset shows the survey location off the coast of Australia

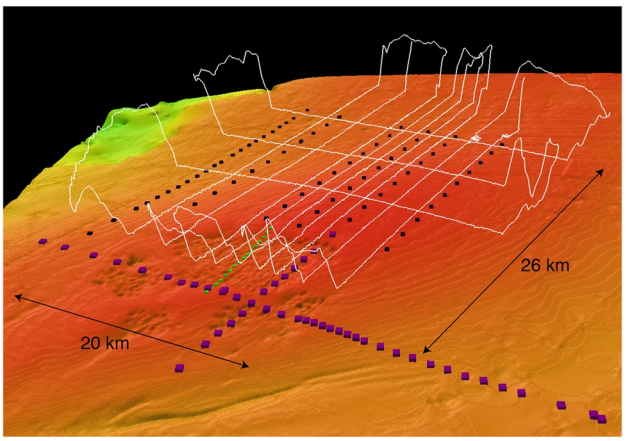

Fig. 13 Perspective view of the ILBL navigation results for the Scarborough gas field survey. White lines show the navigated positions and depths of the deep-towed CSEM transmitter. Colored symbols show the locations of the OBEM receiver array. Orange shading shows seafloor depths of about 900–950 m. Note that the deep-tow is raised to shallower depths for safety during ship turns

Conclusions

We developed an ILBL navigation system and demonstrated it works well to at least 5 km tow depth of the transmitter and receiver array, which is the maximum tested depth. Survey examples show the system can obtain raw position uncertainties of 5 m and 37 m in the inline and crossline directions at 3 km tow depth and 6 m uncertainty at 1 km tow depth. Stacking the raw positions through averaging can be used to further decrease uncertainty. The surface-towed paravane transponders are relatively small and can readily be deployed from any deep-tow capable vessel, while the deep-tow mounted acoustic transceiver system requires dedicated power and telemetry through the tow cable. Unlike USBL systems, the ILBL approach does not require precision installation of sensors nor the dedicated use of ship time to calibrate the system.

The system as described here has proven to work well for our CSEM survey needs and it could readily be adapted for other deep-tow applications requiring precise navigation such as sonar, seismic, magnetic and photographic surveying systems, as well as for deep-towed water column sampling and sensing systems. The accuracy of the current ILBL system could be further improved through several modifications. The paravane GPS receivers could

be replaced with differential receivers. Precision acoustic transponders and transceiver systems could be developed for more precise travel time measurements. While the current ILBL system uses only two transponders towed on paravanes, extra surface transponders could be used to collect additional range measurements that would reduce uncertainties in the navigated deep-tow positions; these additional transponders could be deployed on either additional paravanes, the survey vessel or autonomous surface vessels. Autonomous surface vessels could offer the advantage of being adaptively positioned about the deep-tow vehicle for the optimal normalized aperture and layback for the variable water depths encountered over a survey. The deep-tow ILBL implementation could be used for real-time navigation in addition to the post-processing solutions shown here. The system could also be adapted to navigate autonomous underwater vehicles incorporating the acoustic transceiver system.

Acknowledgements We thank the engineers and technicians in the Scripps Marine EM lab for assistance developing and testing the ILBL system. The Middle America Trench survey was funded by National Science Foundation award OCE-0841114, the San Nicolas Basin survey by Fugro, and the Scarborough project by BHP Billiton Petroleum. We thank Katrin Schwalenberg and an anonymous reviewer for their helpful suggestions.

References

Aster RC, Borchers B, Thurber CH (2019) Parameter estimation and inverse problems, 3rd edn. Elsevier, Amsterdam

Attias E, Weitemeyer K, Hölz S, Naif S, Minshull TA, Best AI, Haroon A, Jegen-Kulcsar M, Berndt C (2018) High-resolution resistivity imaging of marine gas hydrate structures by combined inversion of CSEM towed and ocean-bottom receiver data. Geophys J Int 214(3):1701–1714

Chesley C, Key K, Constable S, Behrens J, MacGregor L (2019) Crustal cracks and frozen flow in oceanic lithosphere inferred from electrical anisotropy. Geochem Geophys Geosyst 20(138):5979–5999

Constable S (2013) Review paper: Instrumentation for marine magnetotelluric and controlled source electromagnetic sounding. Geophys Prospect 61:505–532

Constable S, Cox CS (1996) Marine controlled-source electromagnetic sounding, 2. The PEGASUS experiment. J Geophys Res Solid Earth 101(B3):5519–5530

Constable S, Srnka LJ (2007) An introduction to marine controlled-source electromagnetic methods for hydrocarbon exploration. Geophysics 72(2):WA3–WA12

Constable S, Kannberg PK, Weitemeyer K (2016) Vulcan: a deep-towed CSEM receiver. Geochem Geophys Geosyst 17(3):1042–1064

Cox CS, Constable SC, Chave AD, Webb SC (1986) Controlled-Source electromagnetic sounding of the oceanic lithosphere. Nature 320(6057):52–54

Ellingsrud S, Eidesmo T, Johansen S, Sinha MC, MacGregor LM, Constable S (2002) Remote sensing of hydrocarbon layers by seabed logging (SBL): results from a cruise offshore Angola. Lead Edge 21:972–982

Evans RL, Constable SC, Sinha MC, Cox CS, Unsworth MJ (1991) Upper crustal resistivity structure of the East Pacific Rise near 13° N. Geophys Res Lett 18:1917–1920

Gagnon K, Chadwell CD, Norabuena E (2005) Measuring the onset of locking in the Peru-Chile trench with GPS and acoustic measurements. Nature 434(7030):205–208

Gehrmann RAS, Haroon A, Morton M, Djanni AT, Minshull TA (2019a) Seafloor massive sulphide exploration using deep-towed controlled source electromagnetics: Navigational uncertainties. Geophys J Int 220:1215–1227

Gehrmann RAS, North LJ, Graber S, Szitkar F, Petersen S, Minshull TA, Murton BJ (2019b) Marine mineral exploration with controlled source electromagnetics at the TAG hydrothermal field, 26° N Mid-Atlantic Ridge. Geophys Res Lett 46(11):5808–5816

Gustafson C, Key K, Evans RL (2019) Aquifer systems extending far offshore on the U.S. Atlantic margin. Sci Rep 9(1):1–10

Johansen SE, Panzner M, Mittet R, Amundsen HEF, Lim A, Vik E, Landro M, Arntsen B (2019) Deep electrical imaging of the ultraslow-spreading Mohns Ridge. Nature 567:379–383

Kannberg PK, Constable S (2020) Characterization and quantification of gas hydrates in the California Borderlands. Geophys Res Lett 47(6):1–8

Key K (2009) 1D inversion of multicomponent, multifrequency marine CSEM data: methodology and synthetic studies for resolving thin resistive layers. Geophysics 74(2):F9–F20

Key K, Constable S, Matsuno T, Evans RL, Myer D (2012) Electromagnetic detection of plate hydration due to bending faults at the Middle America Trench. Earth Planet Sci Lett 351–352:45–53

MacGregor LM, Constable S, Sinha MC (1998) The RAMESSES experiment III: Controlled-source electromagnetic sounding of the Reykjanes Ridge at 57°45'N. Geophys J Int 135:773–789

MacGregor LM, Sinha M, Constable S (2001) Electrical resistivity structure of the Valu Fa Ridge, Lau Basin, from marine controlled-source electromagnetic sounding. Geophys J Int 146:217–236

Micallef A, Person M, Haroon A, Weymer BA, Jegen M, Schwalenberg K, Faghih Z, Duan S, Cohen D, Mountjoy JJ, Woelz S, Gable CW, Averes T, Tiwari AK (2020) 3D characterisation and quantification of an offshore freshened groundwater system in the Canterbury Bight. Nat Commun 11(1):1–15

Myer D, Constable S, Key K, Glinsky ME, Liu G (2012) Marine CSEM of the Scarborough gas field, Part 1: Experimental design and data uncertainty. Geophysics 77(4):E281–E299

Myer D, Key K, Constable S (2015) Marine CSEM of the Scarborough gas field, Part 2: 2D inversion. Geophysics 80(3):E187–E196

Naif S, Key K, Constable S, Evans RL (2015) Water-rich bending faults at the Middle America Trench. Geochem Geophys Geosyst 16(8):2582–2597

Naif S, Key K, Constable S, Evans RL (2016) Porosity and fluid budget of a water-rich megathrust revealed with electromagnetic data at the Middle America Trench. Geochem Geophys Geosyst 17(11):4495–4516

Russell JB, Eilon Z, Mosher SG (2019) OBSrange: A new tool for the precise remote location of ocean-bottom seismometers. Seismol Res Lett 90(4):1627–1641

Schwalenberg K, Haeckel M, Poort J, Jegen M (2010) Evaluation of gas hydrate deposits in an active seep area using marine controlled source electromagnetics: Results from Opouawe Bank, Hikurangi Margin, New Zealand. Mar Geol 272:79–88

Shearer P (2009) Introduction to seismology, 2nd edn. Cambridge University Press, Cambridge

Spiess FN, Chadwell CD, Hildebrand JA, Young L, Purcell GH Jr, Dragert H (1998) Precise GPS/Acoustic positioning of seafloor reference points for tectonic studies. Phys Earth Planet Interiors 108:101–112

Swidinsky A, Edwards RN (2011) Joint inversion of navigation and resistivity structure using a fixed transmitter and a moving, linear receiver array: A preliminary study. Geophys J Int 186(3):987–996
Weidelt P (2007) Guided waves in marine CSEM. Geophys J Int 171(1):153–176
Weitemeyer K, Constable S (2014) Navigating marine electromagnetic transmitters using dipole field geometry. Geophys Prospect 62(3):573–596
Weitemeyer KA, Constable S, Trehu AM (2011) A marine electromagnetic survey to detect gas hydrate at Hydrate Ridge, Oregon. Geophys J Int 187(1):45–62